© American Society for Mass Spectrometry, 2017

J. Am. Soc. Mass Spectrom. (2017) 28:1919–1928
DOI: 10.1007/s13361-017-1704-1

RESEARCH ARTICLE

microMS: A Python Platform for Image-Guided Mass Spectrometry Profiling

Troy J. Comi, Elizabeth K. Neumann, Thanh D. Do, Jonathan V. Sweedler

Department of Chemistry and the Beckman Institute for Advanced Science and Technology, University of Illinois at Urbana–Champaign, Urbana, IL 61801, USA

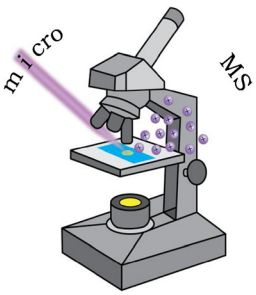

Abstract. Image-guided mass spectrometry (MS) profiling provides a facile framework for analyzing samples ranging from single cells to tissue sections. The fundamental workflow utilizes a whole-slide microscopy image to select targets of interest, determine their spatial locations, and subsequently perform MS analysis at those locations. Improving upon prior reported methodology, a software package was developed for working with microscopy images. microMS, for microscopy-guided mass spectrometry, allows the user to select and profile diverse samples using a variety of target patterns and mass analyzers. Written in Python, the program provides an intuitive graphical user interface to simplify image-guided MS for novice users. The class hierarchy of instrument interactions permits integration of new MS systems while retaining the feature-rich image analysis framework. microMS is a versatile platform for performing targeted profiling experiments using a series of mass spectrometers. The flexibility in mass analyzers greatly simplifies serial analyses of the same targets by different instruments. The current capabilities of microMS are presented, and its application for off-line analysis of single cells on three distinct instruments is demonstrated. The software has been made freely available for research purposes.

Keywords: Image-guided mass spectrometry, Single cell analysis, Software, MALDI, SIMS

Received: 28 March 2017/Revised: 29 April 2017/Accepted: 1 May 2017/Published Online: 7 June 2017

Introduction

Image-guided mass spectrometry (MS) provides a link between the spatial dimensions in a digital image and the physical location of a sample within a microprobe system. MS imaging (MSI) is a subset of image-guided chemical sampling that frequently utilizes regularly spaced acquisition positions overlaid on an optical scan to recreate the spatial distribution of analytes within a sample. However, the widely used rastered MSI approach is low throughput and less sensitive than targeted profiling when analytes (e.g., biological cells and bacterial colonies) are widely dispersed or smaller than the microprobe size. Single cell analysis with MS has attracted great interest due to its sensitivity and ability to handle volume-limited samples [1–6]. Many classes of biomolecules within individual cells are detectible with a variety of MS probes, facilitating new discoveries of single cell heterogeneity and a better understanding of the relationship between chemical contents and cellular functions. When MSI is applied to examine tissue sections [7–10], the resolution to differentiate neighboring cells requires sampling each cell multiple times, effectively splitting available analytes among pixels. Owing to difficulties in sample preparation and stringent instrument requirements, matrix-assisted laser desorption/ionization (MALDI)-MSI at or below single cell resolution is far from routine in most laboratories. Even with secondary ion mass spectrometry (SIMS) imaging, where subcellular resolution is regularly accessible, analysis of a small tissue specimen is often time-consuming. In the case of dispersed cells [11, 12], rastered MSI is not an optimal approach as most of the measurement time is spent characterizing the space between the cells. The limitations of MSI for high-throughput analysis of single cells have led to the development of new methods to locate or deposit cells.

Recently, high-throughput approaches to single cell MS have driven analyses of dissociated single cells that are either chemically labeled [13] or coordinate registered [14]. MS profiling of adhered cells provides advantages in data fusion

Electronic supplementary material The online version of this article (doi:10.1007/s13361-017-1704-1) contains supplementary material, which is available to authorized users.

Correspondence to: Jonathan Sweedler; *e-mail:* jsweedle@illinois.edu

by simplifying data processing and allowing sequential analysis of the same cell. Microarrays for mass spectrometry [15–17] (MAMS) have demonstrated such capabilities by combining Raman microspectroscopy with MS [18]. As an alternative to MAMS, cells may be randomly seeded on a substrate, greatly relaxing fabrication requirements, but at the expense of a necessarily gentle sample extraction. We recently presented such an approach by locating single cells on an indium tin oxide (ITO)-coated glass slide based on their position in a whole-slide fluorescence microscopy image [14]. An inherent challenge with this initial method was the complex scheme for generating custom geometry files, which required manual interaction through several disjointed pieces of software. To facilitate broader adoption of optically-guided single cell profiling, we sought to streamline the process of directing the MS acquisition with whole-slide microscopy images. The first iteration of an improved workflow utilized a point-based similarity registration scheme, which improved target localization accuracy over the previously reported piece-wise linear transform [19]. User interaction was also simplified, allowing fluid interaction with microscope images through a graphical user interface (GUI). All of the functions required to begin acquiring single cell mass spectra on a Bruker ultrafleXtreme instrument were contained in the single piece of software.

Here we present the first version of a new software package—microMS—to support microscopy-guided MS for a variety of image files and mass spectrometers. The software architecture permits new microprobe instruments to be supported, with only minor modifications to the source code. Virtually any spatially restricted sampling probe capable of precisely recording and moving to a given location can perform the profiling.

First, the unique features of microMS are described, along with the necessary modifications to expand device support for both commercial and customized instruments. We then demonstrate microMS using three MS systems for off-line, targeted profiling of single cells from the mammalian nervous system.

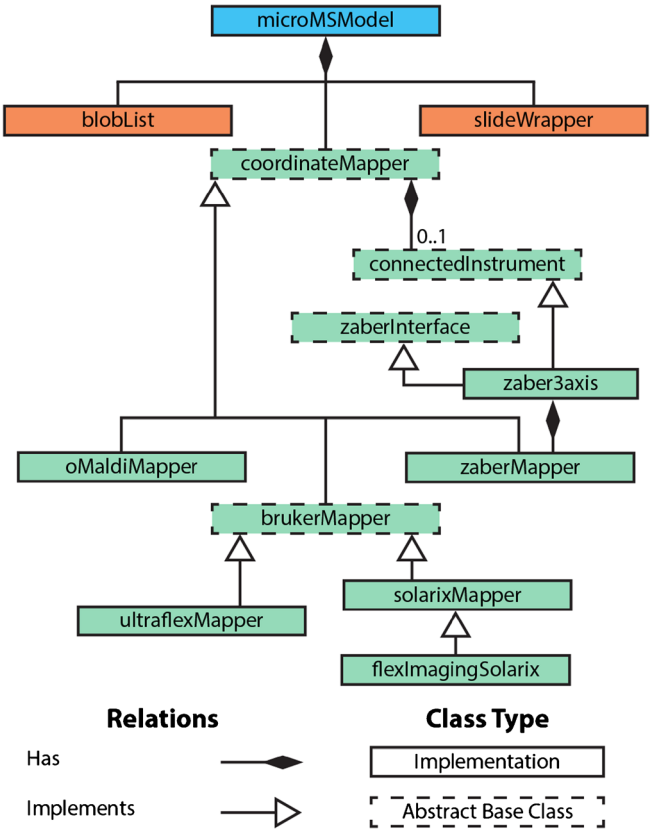

Figure 1. Partial unified modeling language diagram of the microMS class structure. Each experiment is contained in a microMSModel object, consisting of a list of targets (blobList), a microscopy image (slideWrapper), and an instrument mapper (coordinateMapper). The coordinateMapper defines the set of instructions required for each inheriting class. Four concrete instrument implementations are provided with microMS

Experimental

Software

The microMS software is written in Python ver. 3.5. In addition to base components, microMS requires the matplotlib, PyQt5, numpy, scipy, openslide, skimage, and pyserial packages. Installation instructions, usage details, and the source code are included as Supplemental Material. The most recent version and a compiled Windows executable can be downloaded from http://neuroproteomics.scs.illinois.edu/microMS.htm.

The program structure is modeled in the Supplementary Material, Figure S1, with a partial representation in Figure 1. The main GUI class is composed of two widgets in the GUICanvas package; one displays a microscope image and the other displays population-level statistics as a histogram. Each widget interacts with a microMSModel object, which represents a single microscopy experiment (as a blobList and slideWrapper) and mass spectrometer (as a coordinateMapper).

Targets in microMS are represented as objects called "blobs", to generalize a biological cell as any object formed by a group of high-intensity pixels. In Figure 2, there are three blobs, each with a unique Cartesian (x, y) location on the image, a corresponding effective radius, and circularity. The circularity represents the roundness of a blob, scaled between 0 and 1, with 1 being a perfect circle. For example, blobs 1 and 3 are single round cells whereas blob 2 consists of four unresolved cells producing a noncircular blob. A collection of blobs is stored in a blobList object, which also implements methods to query and filter a population of targets.

A slideWrapper provides an object for interacting with a set of microscopy images, representing brightfield and multiple fluorescence channel images. The current field of view is maintained to simplify controller interaction with the image. The ImageUtilities package also contains modules for cell finding, patterning target positions, and optimizing travel paths.

Object models for the MS instruments are contained in the coordinateMappers package, as shown in Figure 1. The

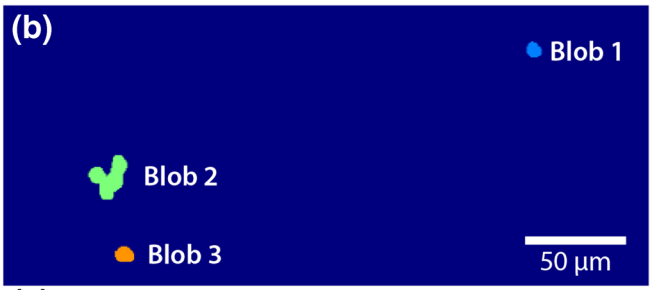

(c)

Blob	X (pix)	Y (pix)	Radius† (pix)	Circularity‡
1	44619	27077	6.79	0.99
2	44241	27192	15.4	0.50
3	44251	27257	7.94	0.98

Figure 2. Overview of blob finding with microMS. (**a**) From an input image, the pixel intensity is filtered by a threshold intensity. (**b**) Pixels above the threshold are grouped with neighboring pixels to generate putative blobs. Each group of pixels is evaluated for its size (in pixels) and circularity and stored within a list, shown as a table in (**c**). The area (*A*) and perimeter (*P*) are directly measured from the threshold image. †The effective radius is calculated as $\sqrt{A/\pi}$. ‡The circularity is calculated as $\frac{4\pi A}{P^2}$

coordinateMapper is an abstract base class providing an interface that the GUI software utilizes to interact with different instrument systems. Abstract base classes define an interface for packages that inherit from them, enforcing implementation of required functions. For object-oriented designs, such interfaces ensure that function calls will succeed without knowing the particular implementation beforehand. The core functionality of the mapper is to align pixel positions with physical coordinates and provide a means to translate target positions on an image to instrument-specific directions. The design of the software architecture simplifies the addition of new instruments. The integration of ambient ionization methods, including single-probe [20–22] or nanospray desorption electrospray ionization [23], are enticing candidates as they have demonstrated single cell sensitivities in imaging and profiling applications. Currently, four specific instrument implementations are supplied in the coordinateMappers package: a Bruker UltrafleXtreme, a Bruker solariX, the AB Sciex oMALDI sample stage attached to a custom hybrid MALDI/C_{60}^+-SIMS, and a lab-built 3-axis liquid microjunction probe. Details about the implementations will be discussed in the Results and Discussion section. Demonstrations for the addition of new instruments to microMS may be found in the microMS User Guide packaged with the source code and supplied here as Supplementary Material.

Chemicals

All chemicals were purchased from Sigma Aldrich (St. Louis, MO, USA) and used without further purification.

Single Cell Dissociation

Two 2–2.5 mo old male Sprague Dawley outbred rats (*Rattus norvegicus*) (www.envigo.com) were housed on a 12-h light cycle and fed ad libitum. Animal euthanasia was performed in accordance with the appropriate institutional animal care guidelines (the Illinois Institutional Animal Care and Use Committee), and in full compliance with federal guidelines for the humane care and treatment of animals. Dissected cerebellum and suprachiasmatic nucleus (SCN) tissues were incubated in a solution of 1% Hoechst 33342 in oxygenated modified Gey's balanced salt solution (mGBSS) for 30 min at 37 °C. The mGBSS solution was removed and the tissues were incubated in an oxygenated solution of 6 units of papain, 1 mM L-cysteine, and 0.5 mM ethylenediaminetetraacetic acid for 80 min at 37 °C. Tissue was then mechanically dissociated in mGBSS with 0.04% paraformaldehyde. A solution of 80% glycerol in mGBSS was added to a final concentration of 40% glycerol. The cell suspension was then transferred onto ITO-coated glass slides (Delta Technologies, Loveland, CO, USA) with at least 12 fiducial marks etched by a diamond-tipped pen.

Microscopy Imaging

Brightfield and fluorescence images were acquired on a Zeiss Axio Imager M2 (Zeiss, Jena, Germany) equipped with an Ab cam Icc5 camera, X-CITE Series 120 Q mercury lamp (Lumen Dynamics, Mississauga, Canada), and a HAL 100 halogen illuminator (Zeiss). The 31000v2 DAPI filter set was used for fluorescence excitation. The images were acquired in mosaic mode with a 10× objective and 13% overlap. Images were processed and exported as tiff files using ZEN software ver. 2 blue edition (Zeiss).

Sample Preparation

Slides were coated with 50 mg/mL 2,5-dihydroxybenzoic acid (DHB) dissolved in 1:1 (v/v) liquid chromatography-grade ethanol:water with 0.1% trifluoroacetic acid with an automatic sprayer as described previously [19, 24]. The matrix solution was supplied at 10 mL/h and nebulized with N_2 gas at 50 psi over 100 passes. Samples were affixed to a rotating plate with the nebulizer positioned 1.5 cm above the samples, resulting in a MALDI matrix thickness of ~0.1–0.2 mg/cm^2.

Instrument Parameters

Single cell analysis was performed on three instruments: (1) An ultrafleXtreme mass spectrometer (Bruker Daltonics, Billerica,

MA, USA), set with a mass window of *m/z* 400–3000. The "Ultra" (~100 μm footprint) laser setting was used with 300 laser shots at 1000 Hz for each cell to generate a MALDI-time-of-flight (TOF) spectrum at each cell. (2) A 7 T solariX Fourier transform-ion cyclotron resonance (FT-ICR) mass spectrometer (Bruker Daltonics), operated with a mass window of *m/z* 150–3000, yielding a 4 Mword time-domain transient. Spectra were calibrated to the phosphatidylcholine head group, $[PC(32:0)+H]^+$, $[PC(34:1)+H]^+$, $[PC(34:1)+Na]^+$, and $[PC(36:1)+Na]^+$, as identified in a separate analysis of cerebellum tissue extract (Table S1). The adsorption mode was used to effectively double the mass resolving power. Each MALDI spectrum was acquired with 20 laser shots at 1000 Hz and 60% laser energy. The laser setting produced an ~100 μm footprint. (3) A custom hybrid MALDI/C_{60}^+ Q-TOF mass spectrometer, described in detail elsewhere [11]. The C_{60}^+ ion beam was utilized for SIMS, with the mass analyzer operated in positive mode with a mass range of *m/z* 60–850. Correctly parsing the spectra requires additional instrument modifications and data analysis routines, described elsewhere [25].

Tentative lipid identifications were made using the Lipid Maps Structure Database (http://www.lipidmaps.org/data/structure/). For the MALDI-FT-ICR mass spectra, a tolerance of ±0.01 Da was used, resulting in sub-ppm mass errors. Intact lipids within the SIMS and MALDI-TOF mass spectra were identified with a tolerance of ±0.2 Da. Putative sodiated lipid adducts were confirmed within the SIMS spectra with tandem MS (Figure S2).

Results and Discussion

Instrument Support in microMS

Bruker instruments are discussed first as their MALDI sample stages and coordinate mappers are similar. The commonality is exploited by the brukerMapper abstract base class, which is a derived class of coordinateMapper; brukerMapper implements methods for reading and writing the xeo geometry files. Xeo files are text-based markup files that provide a sample name and location, as required by Bruker software for automatic acquisition. The brukerMapper class also defines an intermediate coordinate system between physical positions, motor coordinates, and the fractional distances used in xeo files. The classes derived from brukerMapper require a limited set of concrete method implementations to be fully functional, as many features are supported in the bases class. The simplest case is ultraflexMapper, for the Bruker ultrafleXtreme instrument, which defines the required methods to parse user input.

The solarixMapper class for a Bruker solariX instrument is similar to the ultraflexMapper class, with three minor modifications: (1) the xeo files are limited to 400 positions, (2) an xlsx Excel file is also required for automatic acquisition, and (3) input coordinates are read directly from the system clipboard. The flexImagingSolarix object extends solarixMapper and overrides the saved file format for import in flexImaging software. These two instruments provide examples of supporting microscopy-guided MS on Bruker MALDI sources.

Instruments from other vendors inherit directly from the coordinateMapper. One example is the oMALDIMapper for interfacing with an AB Sciex oMALDI server. With this instrument, the sample positions are encoded in ptn pattern files, which are plain text files with tab delimited x,y coordinates relative to the starting position. Hence, in comparison to brukerMapper, oMALDIMapper transforms motor coordinates to ptn coordinates instead of fractional distances. To further simplify the correlation of mass spectra to image coordinates, a corresponding text file with the pixel positions of each target is also exported. As a final consideration, the sample stage was found to have significant backlash upon changing direction. Once measured, the backlash is corrected before exporting the ptn file to ensure accurate targeting.

In the preceding examples, microscopy images are correlated with physical positions on a mass spectrometer sample stage to generate instrument-specific target coordinates. This off-line workflow is ideal for instruments lacking support for external control of the sample stage, as is usually the case. To demonstrate capabilities with on-line analysis and instrument control, additional interfaces were developed for controlling Zaber linear actuators. The zaberMapper class contains a simple implementation of the abstract base class coordinateMapper. It also has an instance variable connectedInstrument, which is used by microMS to interact with the sample stage. Another abstract base class, connectedInstrument, specifies the method signatures necessary for a connected instrument. The concrete implementation provided is a system with three linear actuator stages, zaber3axis. This module inherits from zaberInterface, containing serial wrappers to simplify interaction with each stage, and implements the connectedInstrument interface. During operation, the physical position of the probe is directly read for coordinate registration. The user directs stage movement either by interacting with the optical image or with key strokes.

microMS Functionalities

General features of microMS include locating targets, filtering the target population, patterning each target, and coordinating the image with the physical location of a mass spectrometer stage, as detailed in the subsections below. Only the last step is instrument-specific. Users should refer to the User Guide provided in the Supplementary Material for a comprehensive illustration of these functionalities.

Locating targets Targets may be specified on the microscope image either by manually selecting locations or by performing automatic blob finding. Details of manual target annotation are presented in the provided User Guide. In automatic blob finding, the search takes place over the entire image area unless a region of interest (ROI) is specified. The blob finding algorithm thresholds the specified image color and then groups together pixels above that threshold, as shown in Figure 2b. Each group is then evaluated for its size and circularity. Putative blobs

falling outside the user-specified parameters are discarded. Several features are available to assist with selection of suitable blob finding parameters. Different blob finding parameters are interactively tested on the current image field of view. Additionally, microMS reports pixel intensities, object size, and the circularity of selected positions. Judicious selection of these parameters will find most cells while excluding imaging and background artifacts.

After the targets are located, their properties are stored as lists within microMS. Up to 10 separate target lists are maintained and each list is displayed as a different color. New target sets generated by filtering or patterning are automatically stored in an empty list, with the original target set left intact.

Filtering targets Frequently, it is beneficial to filter the target list, either to refine putative blobs or to stratify targets based on morphology. Basic filtering methods provided by microMS are selected through the menu bar and include ROI filtering and distance filtering. Within a specific ROI, the blobs can be selectively removed or exclusively retained in a new target list. ROI filtering is especially useful for removing targets that are near fiducials or potentially contaminated by substrate background. Distance filtering helps to ensure each MS target position will correspond to a unique object (e.g., a single cell). An appropriate value for distance filtering is chosen based on the microprobe size, target accuracy, and the desired number of samples per blob. For example, a 100-μm diameter probe on a system with 50-μm target accuracy would require distance filtering of at least 100 μm to minimize the chance of sampling a nearby blob. During distance filtering, any target with a neighbor closer than the specified value is removed from the blob list.

In addition to common filtering functions, microMS supports interactive examination of population-level statistics through the histogram window to partition the target list (Figure 3). Metrics include blob size, circularity, nearest neighbor distance, and fluorescence intensity. Note that there is some redundancy between histogram filtering and blob finding. The overlap permits the selection of lenient blob finding parameters to exhaustively identify all putative cells, which are then refined to the final target set. Such a scheme allows distance filtering to identify possible contaminating objects and sub-classifications based on size.

High- and low-pass filters of the targets may be defined on the histogram window. Targets falling within a filter range are dynamically displayed on the microscope image in the corresponding color (Figure 3b, c). Selecting a blob in the microscope image highlights its value on the histogram to assist with defining filter limits. High- and low-pass filters define new target lists that may be further refined by additional histogram operations. This function allows operations such as filtering a population based on size, followed by selection of targets with a particular fluorescent stain. More routinely, the histogram provides a simple method to identify and remove artifacts from blob finding. Figure 3c shows an example of isolating unresolved cells, which helps to ensure data quality.

Patterning targets By default, microMS generates one acquisition target per blob, which is sufficient when the microprobe size is similar to or larger than the target object. However, when the object is larger than the probe, a single acquisition is insufficient to robustly sample heterogeneous objects. Alternatively, MSI of each blob can be acquired at each target location. To address advanced sampling requirements, microMS provides three sample patterning schemes, shown in Figure S3.

The first option is a rectangular packed array of points centered on the target (Figure S3A). Users select a raster spacing and the number of layers to define the overall size of the image. Alternatively, the size is dynamically adjusted to the target radius to ensure complete sampling of heterogeneously sized populations. The resulting data is directly interpretable as an MS image using common MSI software.

Similar to rectangular packing is the hexagonal close packing pattern (Figure S3B). With a circular desorption probe, the hexagonal packing provides denser sampling of the target. Users define the target separation and number of layers, and specify dynamic layering. Although hexagonally packed data are more difficult to reconstruct into an image, averaging the spectra yields a representative spectrum for the blob.

Finally, the circular pattern generates targets around the circumference of each blob (Figure S3C). In some cases, analyzing the center of a blob produces low sensitivity due to the morphology of the target or the biological nature of the samples. Instead, targets are placed immediately outside of a blob to acquire representative spectra. For circular patterning, the user defines a minimum target-to-target distance, maximum number of targets, and offset from the circumference. The actual number of targets around a blob is determined by the blob size and the specified offset while maintaining the target-to-target distance above the minimum limit. Targets are then equally spaced around the blob. Averaging the resulting data provides a characteristic spectrum of the area directly surrounding each blob.

Coordinate transformation to instrument systems Once all targets are determined, the pixel positions must be translated into the physical coordinates of a mass spectrometer or similar platform. Image correlation in microMS is accomplished through a point-based similarity registration. In point-based registration, the target localization error scales inversely with the square root of the number of fiducial points. As such, although microMS supports arbitrary numbers of fiducials, at least 12 fiducials are recommended for robust coordinate training. Similarity transformations do not correct for shearing of images, so the field of view must remain normal to the sample surface during image acquisition and MS analysis.

Generally, a fiducial is located in the microscope image and the instrument system with the assistance of an integrated video

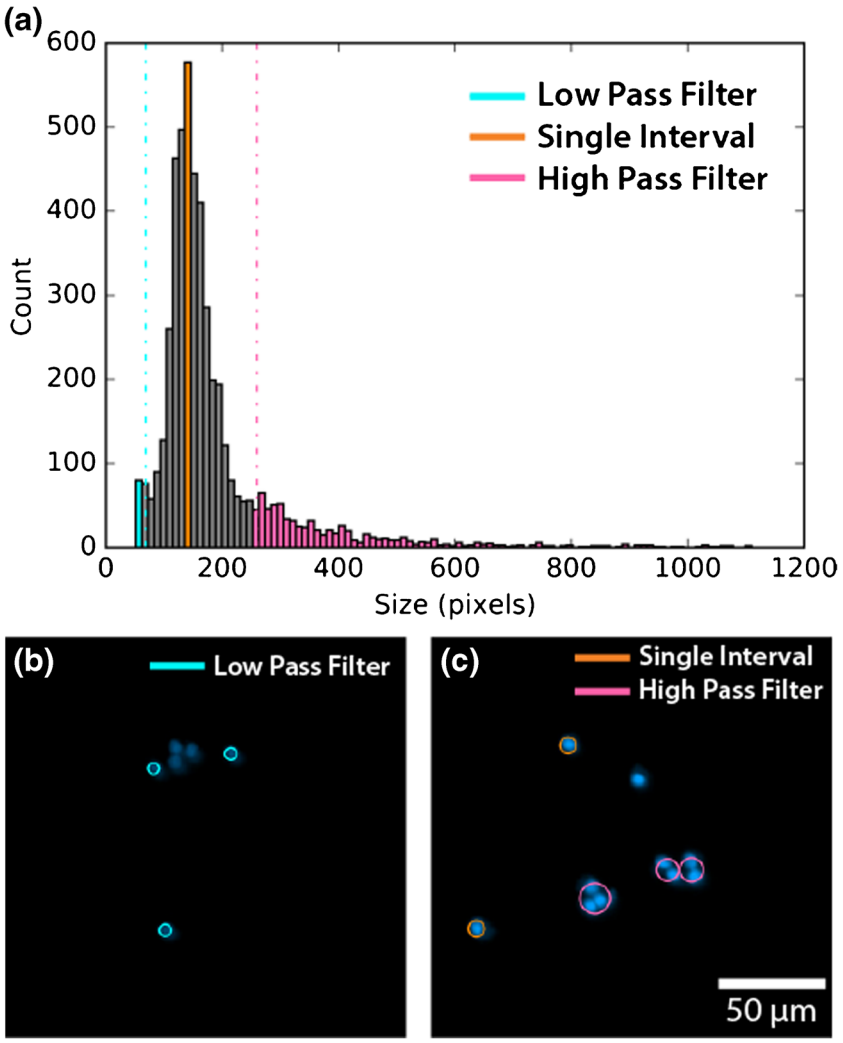

Figure 3. Population-level filtering through the histogram window. (**a**) A population of found blobs may be filtered by size, circularity, minimum pairwise distance, or fluorescence intensity; (**b**) and (**c**) the histogram can be divided into a low-pass, high-pass, or single interval, with the appropriate blobs dynamically colored in the microscope image

camera. When the microprobe is positioned over the center of a fiducial mark, the same location is selected on the image in microMS. This opens a popup window requesting the physical *x, y* position. A default *x, y* position is displayed in the popup that directly reads the stage position, pastes text from the computer clipboard, or predicts the closest location, depending on the selected instrument.

Fiducials are displayed on the microscope image as blue circles with labels corresponding to the nearest set position on the instrument, as shown in the schematic in Figure 4. A few feedback features are included to help the user assess the quality of the current registration. If applicable, labels display set points of the instrument coordinate system. The labels shown in Figure 4b correspond to a Bruker MTP slide II adapter. For some instruments, a set of preprogrammed positions are displayed, showing the predicted location of those points on the microscope image. A large deviation, typically attributable to an inaccurate input, will be detected by a discrepancy in the expected and displayed label. Finally, the fiducial with the worst fiducial localization error is highlighted in red, indicating that specific position assignment should be reconsidered. Correcting the problematic fiducial will cause the next worst fiducial to be highlighted. Once the same fiducial stays highlighted, the registration is close to optimal. Adjusting the worst fiducial is good practice to produce accurate targets.

With a full set of fiducials, the target positions may be saved in instrument-specific format for offline analysis. Alternatively, microMS can communicate directly with an instrument to instruct it to move and perform an analysis. Owing to limited vendor support, direct instrument control is implemented only for a lab-built liquid microjunction extraction probe, which will be described in a follow-up publication.

The current microMS distribution supports the Bruker ultrafleXtreme, Bruker solariX, AB Sciex oMALDI server, and a lab-built liquid microjunction extraction stage. For the supported MS systems, the user registers fiducials and saves instrument positions without modifications. Furthermore, microMS has ample room for customization due to the abstract

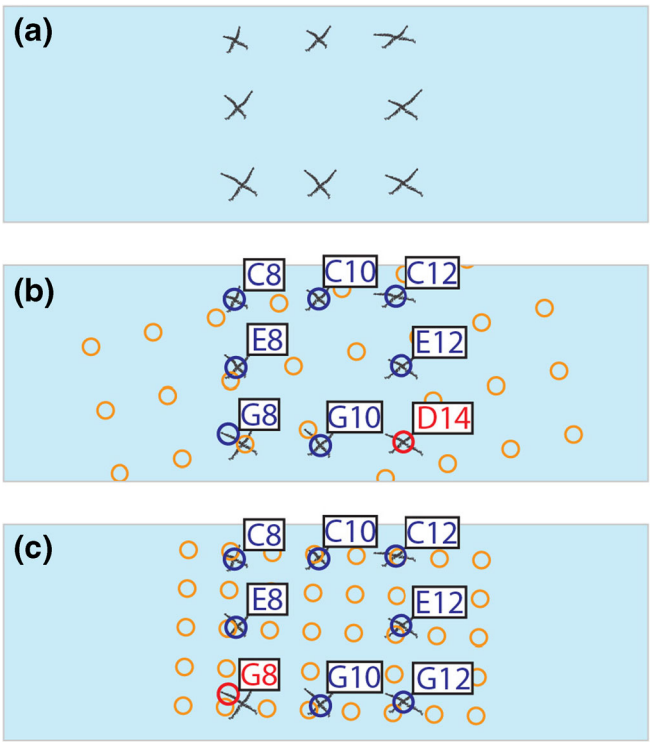

Figure 4. Schematic of fiducial training. (**a**) The input image includes several fiducial points, such as etched x marks on the glass slide. (**b**) An initial attempt at registration with labels of the nearest named coordinate for each fiducial. Fiducials are shown in blue, except the point with the worst fiducial localization error, which is in red. A set of predicted locations in yellow are also be displayed. (**c**) After removing and retraining the worst fiducial, the next worst fiducial is dynamically highlighted

base class construction of the CoordinateMappers package. The general framework remains unchanged, but there are opportunities to tune each function to a specific application. Examples include the ability to directly read fiducial positions from an instrument, grab the contents of the computer clipboard, and perform stage movement backlash correction.

Accuracy of Point-Based Similarity Registration

A vital metric for optically guided profiling is the target localization error. An accurate transformation between the optical image and physical location ensures that each sample corresponds to the position of interest. Including more fiducials reduces target localization errors, effectively distributing the uncertainty of a given fiducial over the entire transformation. Several factors influence accuracy: the precision of stage movement, fiducial localization accuracy (in both image and physical coordinate systems), number of fiducials, whole-slide image stitching, and proper sample positioning during image and MS acquisition. Users should carefully consider these factors in order to establish adequate probe size and distance cutoffs prior to data acquisition.

To assess the accuracy of an MS system with microMS, an image-based method was developed to link the requested and actual target positions, as shown in Figure 5. The target localization error is defined as the Euclidean distance between a requested position and the actual, transformed position during coordinate registration, and is synonymous with accuracy. To assess this value, a thin layer of DHB matrix was coated on an ITO glass slide to act as a tracer for the probe position. A standard sample was prepared with 16–24 fiducials along the exterior of a target. An additional set of fiducials was included within this region to mimic the location of samples in a profiling experiment. The interior marks were not used for coordinate registration, but rather, to assist with overlaying the pre- and post-analysis images. Several target locations were manually placed around each interior fiducial. Dividing the targets between multiple trials is useful for designing experiments to test the effects of possible confounding variables.

Next, fiducial training was performed with the MS system and the set of targets was desorbed with sufficient time to noticeably remove the DHB matrix. After desorption, the target area was optically imaged again to reveal the actual position of sampling events. Desorption locations and sizes were marked as blobs in microMS and saved for further analysis. To overlay the two images, subsets of the pre- and post-desorption images were cropped and roughly positioned prior to intensity-based registration with custom scripts in MATLAB (R2015b). The resulting transformation was used to map the target pixel positions onto the post-extraction image. The distance between the requested and actual desorption positions is a direct measurement of the target localization error. With this method, the target localization of the Bruker ultrafleXtreme was found to be 38.3 ± 3.9 µm (mean ± S.E.M, n = 71, Figure 5), whereas the liquid microjunction extraction stage accuracy was 42.8 ± 2.3 µm (n = 48; data not shown) over an area of approximately half a microscope slide, an error of about one part per thousand. As previously mentioned, the probe radius should be as large as the target localization error, and the distance filter applied should be larger than the sum of this error and the probe radius.

In experiments to assess the effects of various confounding factors on target accuracy, desorption was repeated multiple times with the same sample and slide image. Different laser spot sizes, users, target locations, and fiducial training sets were examined. The only significant factor found was the fiducial training set (Figure 5d). Overall accuracy is not dependent on the target location (Figure 5e), laser spot size, or user (data not shown). Within an experiment, the accuracy is fairly constant, independent of the user or location on the sample. However, repeating an experiment with the same sample could produce significantly different accuracy. This result confirms the profound effect of quality fiducial training sets on the target accuracy. Extreme care is required when training fiducials to

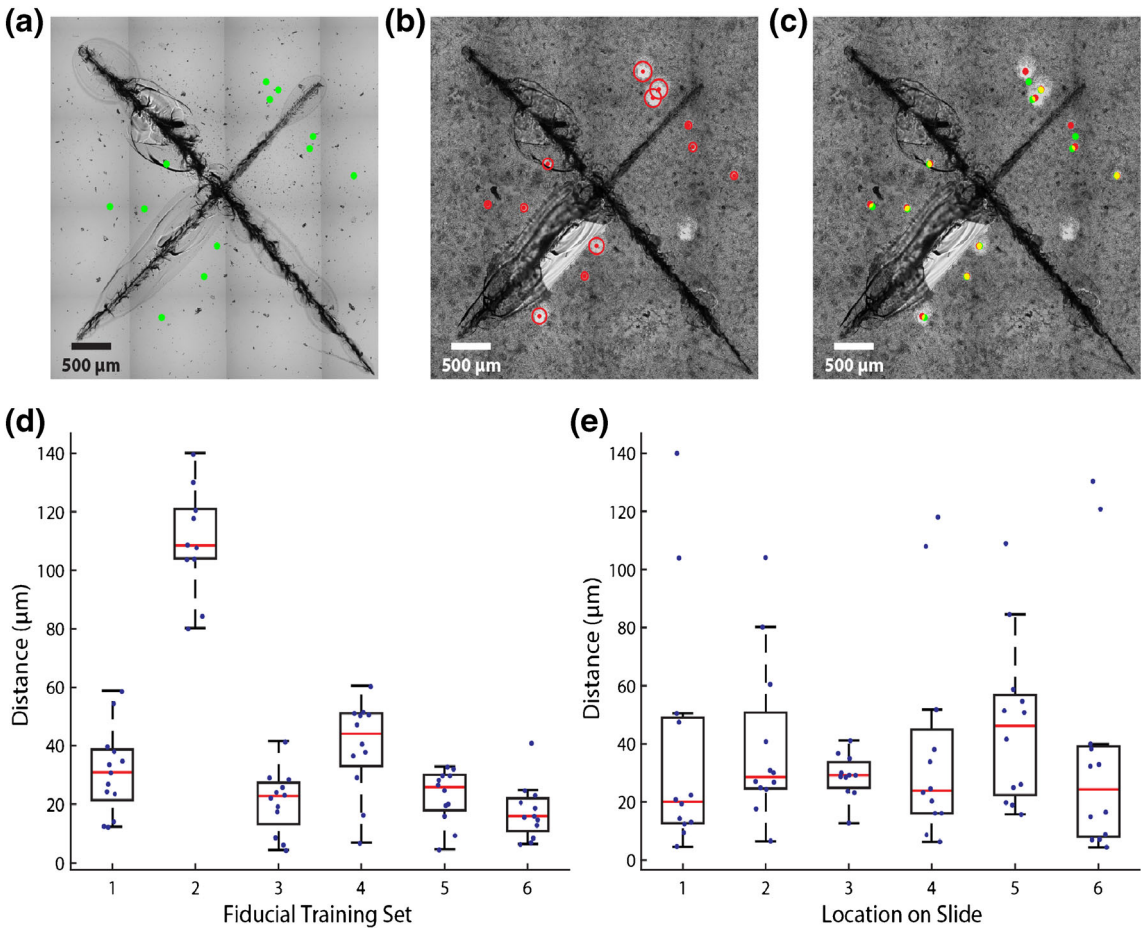

Figure 5. Determination of target localization errors. (**a**) Target locations (green) are marked around an image of an etched x mark. The sample is then coated with a thin layer of MALDI matrix and analyzed by optically guided MS to generate desorption craters in the matrix. (**b**) The location of resulting desorption events (red) are determined by optical microscopy. (**c**) Image registration of panels A and B allows the direct mapping of requested target locations onto the desorption marks. Overlap is shown in yellow. The distance between these positions is the target localization error of the registration set. The effect of various parameters may be assessed simultaneously including multiple training sets, location on slide, or size of microprobe, as shown here. A three-way linear ANOVA demonstrated that while the specific fiducial training set significantly affected (**d**) accuracy ($p << 0.05$), and (**e**) the location on the slide ($p = 0.6$), it did not significantly affect spot size ($p = 0.3$, not shown)

ensure the image target locations correspond to the expected mass spectra.

A Demonstration: Sequential Analysis of the Same Target

For single cell profiling experiments, the physical location of a cell on the slide effectively isolates it from neighbors and prevents mixing, which greatly simplifies data fusion. microMS provides a utility for performing sequential analysis of the same target on different instruments with ease. Using the optical image as a map to record each target address, the image position can be transformed into any supported instrument coordinate system. A careful selection of the order of experiments facilitates the repeated analysis of a sample to provide complementary chemical information.

Figure 6 shows two examples of sequential single cell profiling using MS instruments with different capabilities. In Figure 6a, dispersed rat cerebellum cells were initially profiled with a Bruker ultrafleXtreme to rapidly assess the lipid content, with moderate resolution and mass accuracy. From the initial mass spectral dataset, cells without significant lipid signals are discarded from further consideration as they likely represent artifacts from optical imaging or sample preparation, such as dust particles. The resulting population is then selected for follow-up, high resolution, high mass accuracy analysis with a Bruker solariX FT-ICR. Owing to the increased sample acquisition time, exhaustive analysis of large populations is cost-prohibitive. Performing a preliminary filtering step maximizes the efficiency of subsequent data analysis, without consuming the entire cellular content.

Although the overall lipid profiles are similar, there are some discrepancies between the lipid ratios obtained with the two methods. This could represent changes in the sample layers that each technique is analyzing. Nonetheless, the advantage of single cell FT-ICR MS is immediately apparent with the ppm

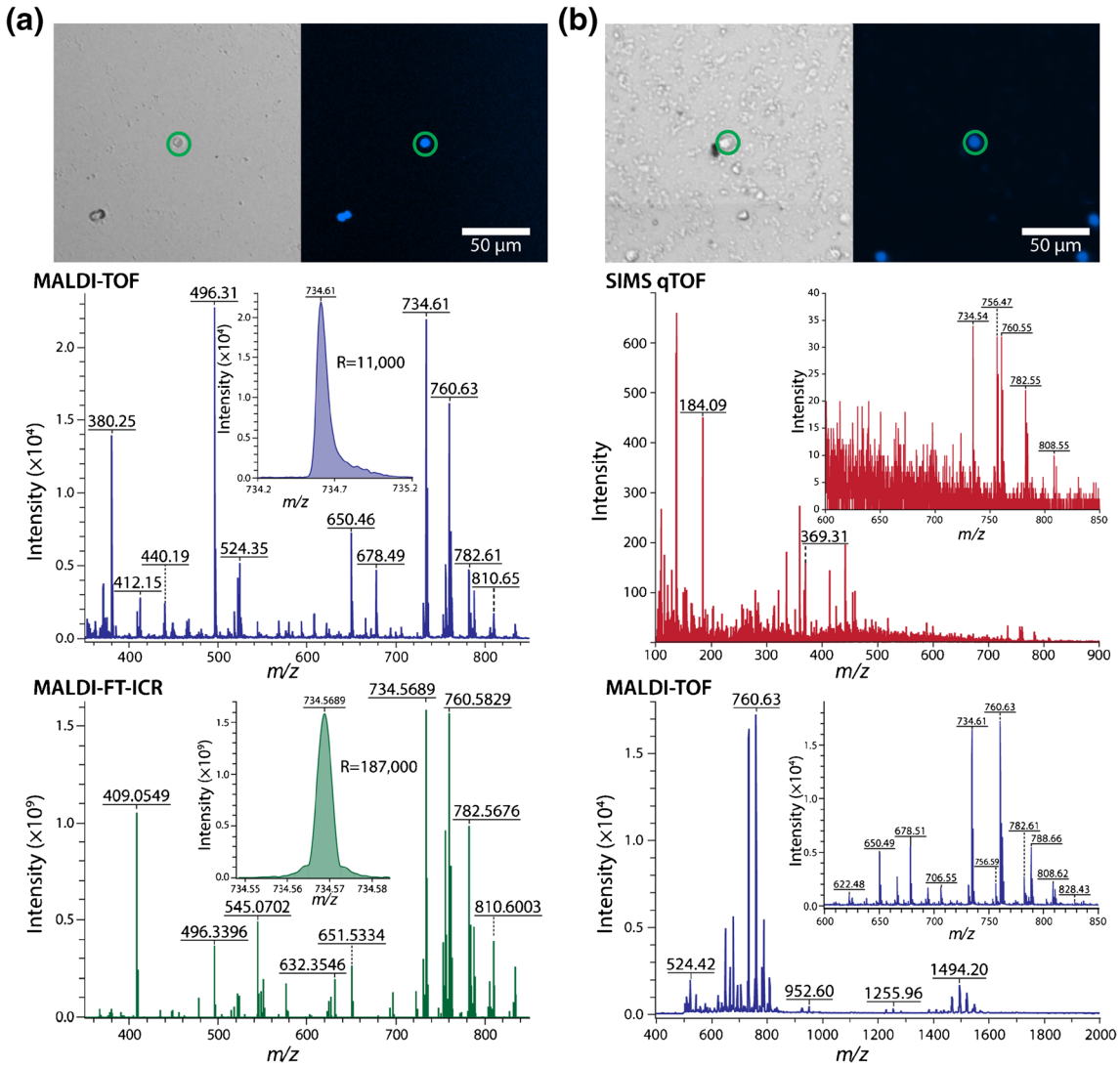

Figure 6. Sequential analysis of the same cell with two separate MS systems. Once a cell has been located in the optical image (top), its location remains fixed through multiple analyses, allowing two instruments to probe the same set of selected cells. (**a**) MALDI-TOF MS (middle) of a cerebellum-derived cell followed by MALDI-FT-ICR MS (bottom). MALDI-TOF MS provides high throughput screening of thousands of cells to highlight rare or representative individuals. Here, FT-ICR MS provides high mass resolution and high mass accuracy for unequivocal elemental composition of selected cellular contents. (**b**) SIMS profiling (middle) followed by MALDI-TOF MS (bottom) with a DHB-coated, SCN-derived cell. SIMS provides information on small molecule compounds, whereas MALDI-TOF MS effectively detects larger species, such as lipid dimers and peptides. The inset demonstrates some overlap of intact lipid coverage from each modality

mass accuracy and over an order of magnitude higher mass resolution, shown in each inset for putative $[PC(32:0)+H]^+$ (Figure 6a). Once the MALDI-TOF analysis has identified cells with abundant lipid signals, they are filtered to locate individuals requiring exact mass measurement for elemental composition analysis. Such a workflow facilitates exhaustive cell population analysis while efficiently utilizing the FT-ICR instrument as needed.

As a second example, Figure 6b displays a C_{60}^+-SIMS mass spectrum and the corresponding MALDI-TOF mass spectrum of a single cell derived from the rat SCN. Here, the low sample consumption of SIMS was leveraged by follow-up MALDI-TOF MS to provide greater, complementary information than would be possible with either technique alone. In the low mass range, peaks corresponding to the phosphatidylcholine head group and a cholesterol fragment are apparent in the SIMS spectrum at *m/z* 184.09 and 369.31, respectively. The MALDI-TOF instrument demonstrates better sensitivity to intact lipids, and detects lipid dimers and peptides. Comparing the identity of the lipids over the same range, SIMS appears to favor sodiated adducts ($[PC(32:0)+Na]^+$ and $[PC(34:1)+Na]^+$ at *m/z* 756.47 and 782.55, respectively) more than the protonated forms seen in the MALDI-TOF results ($[PC(32:0)+H]^+$ and $[PC(34:1)+H]^+$ at *m/z* 734.54 and 760.55, respectively). These

relative intensities likely reflect the different ionization processes occurring in each instrument. Together, a wide mass range is covered to provide a more complete profile of the sample.

These examples may represent the first demonstration of multiple MS platforms used to measure the same individual cells with high throughput. In each example, the ability to repeatedly analyze the same cell was leveraged to acquire complementary information from more than one instrument. Such an experiment would be difficult to perform at high throughput without linking the target locations with the optical image of each sample. With microMS, sequential analysis is facile, enabling each cell to be exhaustively characterized by multiple techniques.

Conclusions and Future Directions

microMS is the first generation of an open source Python package for robust image analysis and coordinate registration, which are essential for optically-guided MS profiling. microMS provides a rich feature set for image analysis that is suited for optically-guided MS profiling. Targets may be automatically located, filtered, stratified, and patterned prior to MS analysis. These functions provide access to single cell profiling with multichannel fluorescence image analysis. The unique aspect of microMS is how mass spectrometers are represented for MS profiling. The implementation of specific MS systems through an abstract base class and software architecture provides a straightforward means for adapting microMS to arbitrary microprobe instruments. While this simplifies connecting microMS to new systems, it also facilitates sequential analysis of the same target by uniquely addressing each cell coordinate. We believe the rich feature set and ease of extending microMS to a variety of mass spectrometers and other instruments will facilitate the growth of single cell profiling.

Acknowledgements

The authors thank Stanislav Rubakhin for assistance with sample preparation, and Tong Si for useful discussions. They also gratefully acknowledge support from the National Institutes of Health, Award Number P30 DA018310 from the National Institute on Drug Abuse, and from the National Institute of Mental Health, Award Number 1U01 MH109062. T.J.C. and E.K.N. acknowledge support from the National Science Foundation Graduate Research Fellowship Program and the Springborn Fellowship. T.J.C. received additional support through the Training Program at Chemistry-Interface with Biology (T32 GM070421).

References

1. Lanni, E.J., Rubakhin, S.S., Sweedler, J.V.: Mass spectrometry imaging and profiling of single cells. J. Proteom. **75**, 5036–5051 (2012)
2. Rubakhin, S.S., Lanni, E.J., Sweedler, J.V.: Progress toward single cell metabolomics. Curr. Opin. Biotechnol. **24**, 95–104 (2013)
3. Comi, T.J., Do, T.D., Rubakhin, S.S., Sweedler, J.V.: Categorizing cells on the basis of their chemical profiles: progress in single-cell mass spectrometry. J. Am. Chem. Soc. **139**, 3920–3929 (2017)
4. Armbrecht, L., Dittrich, P.S.: Recent advances in the analysis of single cells. Anal. Chem. **89**, 2–21 (2017)
5. Chen, X., Love, J.C., Navin, N.E., Pachter, L., Stubbington, M.J.T., Svensson, V., Sweedler, J.V., Teichmann, S.A.: Single-cell analysis at the threshold. Nat. Biotech. **34**, 1111–1118 (2016)
6. Zenobi, R.: Single-cell metabolomics: analytical and biological perspectives. Science **342**, 1243259 (2013)
7. Korte, A.R., Yandeau-Nelson, M.D., Nikolau, B.J., Lee, Y.J.: Subcellular-level resolution MALDI-MS imaging of maize leaf metabolites by MALDI-linear ion trap-Orbitrap mass spectrometer. Anal. Bioanal. Chem. **407**, 2301–2309 (2015)
8. Kompauer, M., Heiles, S., Spengler, B.: Atmospheric pressure MALDI mass spectrometry imaging of tissues and cells at 1.4-μm lateral resolution. Nat. Methods **14**, 90–96 (2017)
9. Lee, J.K., Jansson, E.T., Nam, H.G., Zare, R.N.: High-resolution live-cell imaging and analysis by laser desorption/ionization droplet delivery mass spectrometry. Anal. Chem. **88**, 5453–5461 (2016)
10. Passarelli, M.K., Ewing, A.G.: Single-cell imaging mass spectrometry. Curr. Opin. Chem. Biol. **17**, 854–859 (2013)
11. Lanni, E.J., Dunham, S.J., Nemes, P., Rubakhin, S.S., Sweedler, J.V.: Biomolecular imaging with a C60-SIMS/MALDI dual ion source hybrid mass spectrometer: instrumentation, matrix enhancement, and single cell analysis. J. Am. Soc. Mass Spectrom. **25**, 1897–1907 (2014)
12. Yeager, A.N., Weber, P.K., Kraft, M.L.: Three-dimensional imaging of cholesterol and sphingolipids within a Madin-Darby canine kidney cell. Biointerphases **11**, 02A309 (2016)
13. Spitzer, M.H., Nolan, G.P.: Mass cytometry: single cells, many features. Cell **165**, 780–791 (2016)
14. Ong, T.H., Kissick, D.J., Jansson, E.T., Comi, T.J., Romanova, E.V., Rubakhin, S.S., Sweedler, J.V.: Classification of large cellular populations and discovery of rare cells using single cell matrix-assisted laser desorption/ionization time-of-flight mass spectrometry. Anal. Chem. **87**, 7036–7042 (2015)
15. Pabst, M., Fagerer, S.R., Kohling, R., Kuster, S.K., Steinhoff, R., Badertscher, M., Wahl, F., Dittrich, P.S., Jefimovs, K., Zenobi, R.: Self-aliquoting microarray plates for accurate quantitative matrix-assisted laser desorption/ionization mass spectrometry. Anal. Chem. **85**, 9771–9776 (2013)
16. Ibáñez, A.J., Fagerer, S.R., Schmidt, A.M., Urban, P.L., Jefimovs, K., Geiger, P., Dechant, R., Heinemann, M., Zenobi, R.: Mass spectrometry-based metabolomics of single yeast cells. Proc. Natl. Acad. Sci. U. S. A. **110**, 8790–8794 (2013)
17. Krismer, J., Sobek, J., Steinhoff, R.F., Fagerer, S.R., Pabst, M., Zenobi, R.: Screening of *Chlamydomonas reinhardtii* populations with single-cell resolution by using a high-throughput microscale sample preparation for matrix-assisted laser desorption ionization mass spectrometry. Appl. Environ. Microbiol. **81**, 5546–5551 (2015)
18. Fagerer, S., Schmid, T., Ibanez, A., Pabst, M., Steinhoff, R., Jefimovs, K., Urban, P., Zenobi, R.: Analysis of single algal cells by combining mass spectrometry with Raman and fluorescence mapping. Analyst 6732–6736 (2013)
19. Jansson, E.T., Comi, T.J., Rubakhin, S.S., Sweedler, J.V.: Single cell peptide heterogeneity of rat islets of Langerhans. ACS Chem. Biol. **11**, 2588–2595 (2016)
20. Pan, N., Rao, W., Kothapalli, N.R., Liu, R., Burgett, A.W., Yang, Z.: The single-probe: a miniaturized multifunctional device for single cell mass spectrometry analysis. Anal. Chem. **86**, 9376–9380 (2014)
21. Rao, W., Pan, N., Yang, Z.: Applications of the single-probe: mass spectrometry imaging and single cell analysis under ambient cconditions. J. Vis. Exp. e53911 (2016)
22. Pan, N., Rao, W., Standke, S.J., Yang, Z.: Using dicationic ion-pairing compounds To enhance the single cell mass spectrometry analysis using the single-probe: a microscale sampling and ionization device. Anal. Chem. **88**, 6812–6819 (2016)
23. Laskin, J., Heath, B.S., Roach, P.J., Cazares, L., Semmes, O.J.: Tissue imaging using nanospray desorption electrospray ionization mass spectrometry. Anal. Chem. **84**, 141–148 (2012)
24. Li, B., Comi, T.J., Si, T., Dunham, S.J., Sweedler, J.V.: A one-step matrix application method for MALDI mass spectrometry imaging of bacterial colony biofilms. J. Mass Spectrom. **51**, 1030–1035 (2016)
25. Do, T.D., Comi, T.J., Dunham, S.J.B., Rubakhin, S.S., Sweedler, J.V.: Single cell profiling using ionic liquid matrix-enhanced secondary ion mass spectrometry for neuronal cell type differentiation. Anal. Chem. **89**, 3078–3086 (2017)